World Ocean Density Ratios

HORACIO A. FIGUEROA*

Atmospheric and Oceanic Sciences Program, Princeton University, Princeton, New Jersey

29 November 1994 and 30 March 1995

ABSTRACT

In this report, the potential for salt finger instability in the central water of the World Ocean is examined. The form of the temperature–salinity relationship determined from the Levitus climatological data and the density ratio of this relationship are used as a proxy to identify the regions that are susceptible to salt finger activity. The analysis indicates that most of the North and South Atlantic basins, and southeastern Indian and southwestern South Pacific Central Waters have density ratios smaller than 2.0. This is an indication that enhanced vertical salinity fluxes due to salt fingers can be an additional process affecting the thermocline freshwater budget. This study also indicates that most of the ocean's central water T–S curves are better described by a constant density ratio T–S curve than by a straight line connecting near-surface and intermediate water types.

1. Introduction

The role played by double diffusive processes in the distribution of temperature and salinity of the world oceans has been studied in the past within the framework of theoretical, experimental, and laboratory work (see Schmitt 1994a). Double diffusive processes occur when at least two components of the fluid have different molecular diffusivities and make opposing contributions to the vertical density gradient (Huppert and Turner 1981).

While double diffusion in the ocean is usually associated with small-scale processes affecting temperature and salinity vertical distributions, there is observational and theoretical evidence that suggests that double diffusive processes can also affect the large-scale distribution of properties in the ocean. Ingham (1966) showed that the form of the temperature and salinity curve of the central waters of the World Ocean could be related to the density ratio (R_ρ) of the temperature–salinity relationship. This ratio is defined as the ratio of the thermal to the haline effect of temperature and salinity changes on the density stratification. Ingham indicated that the form of the central water's T–S curve is better represented by a constant density ratio curve than by a straight line. Schmitt (1981) showed that the central water's T–S relation may be controlled as much by small-scale double diffusive processes as by the atmospheric forcing.

In a series of papers Schmitt (Schmitt and Evans 1978; Schmitt 1981, 1990) concluded that salt finger instabilities were responsible for the form of the central water's T–S curve and that the form of the T–S curve could provide direct evidence of salt finger activity. Furthermore, Schmitt showed that only when $R_\rho < 2.0$ the growth rate of salt finger instabilities is fast enough to result in a distinctive enhancement of the vertical salt flux. Schmitt and Evans (1978) estimated vertical salt fluxes due to salt fingers in the western North Atlantic and concluded that they can be of the same order of magnitude as the freshwater fluxes due to evaporation and precipitation at the surface.

This paper builds upon the work of Ingham (1966) and Schmitt (1981), and extends their calculation to all central waters of the World Ocean. The objective is to present evidence from a global climatological dataset (Levitus 1982) that the temperature and salinity of the World Ocean central waters show a clear tendency to be better represented by a constant density ratio curve than by a linear temperature–salinity curve connecting near-surface and intermediate water masses. Furthermore, we present evidence that there are large oceanic areas where the density ratio of the central waters is smaller than 2, indicating the potential for salt finger instabilities.

2. Density ratio of the World Ocean central waters

The density ratio can be roughly estimated by the ratio of the temperature and salinity differences between the two endmembers defining the central water. The lower endmember is represented by the intermediate waters, while the surface endmember is very

* Current affiliation: Oracle Argentina, Madero 1020, Buenos Aires 1106, Argentina.

Corresponding author address: Dr. Horacio A. Figueroa, Oracle Argentina, Buenos Aires 1106, Argentina.
E-mail: horacio@splash.princeton.edu

much dependent on the local heat and freshwater fluxes and advective velocity field, and is assumed to be below the seasonal thermocline.

Two diagnostics are estimated and discussed in what follows. They are the density ratio (R_ρ) of the central water's temperature–salinity relationship and an "error ratio." The density ratio provides a measure of the potential for salt finger instabilities. The error ratio is the ratio of the squared difference between the observed T–S curve and a constant density ratio T–S curve, and the squared difference between the observed T–S curve and a straight line.

The density ratio (R_ρ) is estimated from the temperature and salinity vertical distribution:

$$R_\rho = \frac{\alpha \Delta T}{\beta \Delta S}, \tag{1}$$

where

$$\alpha = -\frac{1}{\rho}\frac{\partial \rho}{\partial T}$$

and

$$\beta = \frac{1}{\rho}\frac{\partial \rho}{\partial S}$$

represent the thermal expansion and haline contraction coefficients and are obtained from the explicit differentiation of the equation of state (UNESCO 1981). These coefficients depend on temperature, salinity, and pressure. Since we are interested in the central water, located in the upper 1000 m of the water column, the pressure dependence of these coefficients is negligible and therefore not considered in the calculations.

As in Schmitt (1981) and Greengrove and Rennie (1991), the R_ρ corresponding to a given T–S curve is estimated by integrating Eq. (1) as

$$T(S) = T(S_o) + \int_{S_o}^{S} \frac{\beta}{\alpha} R_\rho dS \tag{2}$$

and adjusting R_ρ and $T(S_o)$ so as to minimize the squared difference between the observed T–S relationship and the $T(S)$ obtained from Eq. (2). The central waters are defined here as the waters between the near-surface salinity maximum and the intermediate waters salinity minimum. In the absence of a salinity maxima or minima, an inflection in the T–S curve was used to define the T–S properties of the endmembers.

The Levitus (1982) climatological dataset is used in this study. The data is arranged on a one-degree grid and has 33 levels in the vertical, 21 of which are in the upper 1000 m.

The T–S curve for each 10° × 10° Canadian square is calculated by averaging the Levitus (1982) one-degree climatological temperature and salinity values as

$$\bar{T}(S) = \frac{1}{N}\sum_{i=1}^{i=10}\sum_{j=1}^{j=10} T(S)\delta(S - S'), \tag{3}$$

where $\delta(S - S')$ is 0.05, the salinity bin. That is, temperatures within the central water and $0.05\delta(S - S')$ intervals are averaged to obtain $\bar{T}(S)$; i and j represent the one-degree grid points within each 10° × 10° Canadian square. The $\bar{T}(S)$ obtained this way is the one used to calculate the R_ρ and $\bar{T}(S_o)$ that minimizes the error between the observed T–S and the T–S obtained from Eq. (2).

The second diagnostic used in the analysis of the double-diffusive properties of the World Ocean's Central Water is the ratio of the squared difference between the T–S determined from a constant density ratio [Eq. (2)] and the observations, and the squared difference between a linear fit and the observed T–S:

$$\epsilon = \frac{\epsilon R_\rho}{\epsilon_L} = \frac{\sum_{1}^{N-1}(T_{R_\rho} - T_{obs})^2}{\sum_{1}^{N-1}(T_L - T_{obs})^2}, \tag{4}$$

where N is the number of 0.05 salinity bins corresponding to each $\bar{T}(S)$ curve and T_{R_ρ}, T_{obs}, and T_L are the temperatures as determined from a constant density ratio coefficient, the observed temperature, and the temperature determined from a linear regression, respectively.

In regions where ϵ is smaller than 1, a constant density ratio T–S curve better represents the observed T–S properties than a linear fit to the data. If these regions coincide with regions where $R_\rho < 2$, then it can be argued that salt fingers might play a significant role in controlling the T–S curve of the central waters.

3. Discussion

The temperature and salinity of the World Ocean central water are the result of the combined effect of the geographical distribution of the heat and freshwater fluxes at the air–sea interface, the intensity and location of the wind-driven midocean gyres, and the character of the small-scale diffusive process occurring in the interior. The prevalence of one mechanism over the others will then determine the form of the temperature–salinity relationship.

While the distribution of the surface fluxes is not yet well understood, an approximate description of the large-scale features of the water cycle has recently been presented by Schmitt (1994b), based on an updated version of the Baumgartner and Reichel (1975) evaporation minus precipitation ($E - P$) maps (Fig. 1). The subtropical gyres are characterized by an excess of evaporation, whereas the tropical and subpolar regions show an excess of precipitation (Fig. 1). The region of net precipitation in the North Pacific is significantly larger and extends farther south than in the North Atlantic. The North and South Pacific subtropics are separated by a region of net precipitation just north of the equator associated with the intertropical convergence zone. This rough description of the hydrological cycle

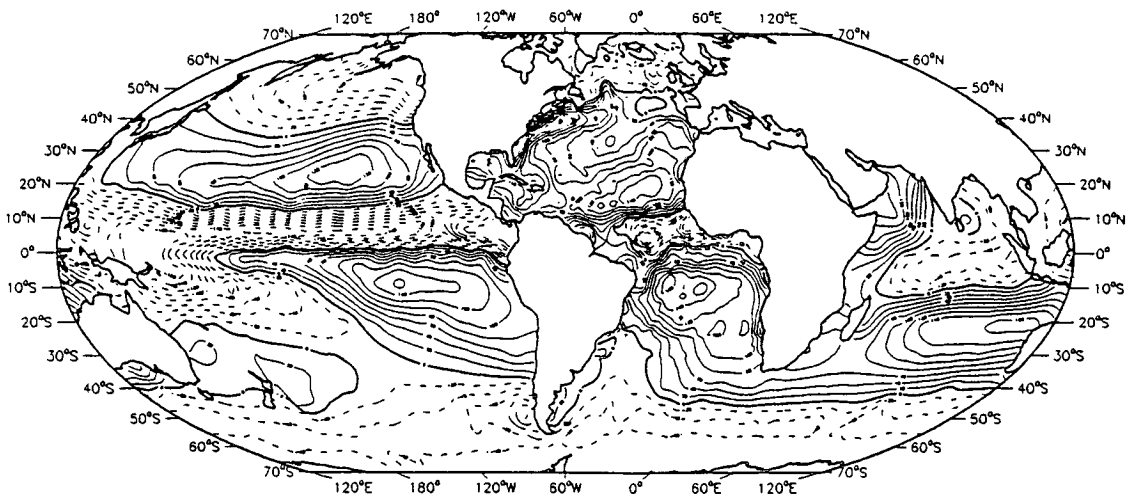

FIG. 1. $E - P$ in (cm/yr) from Schmitt (1994b). Net precipitation is represented by dashed lines.

is consistent with the distribution of the near-surface salinity maximum associated with the subtropical gyres and the salinity minimum characteristic of intermediate waters subducted at higher latitudes.

Temperature and salinities from the Levitus climatology are used to characterize the central water of the World Ocean. Figures 2a–d show the temperature and salinity fields at the depth of the salinity maximum and the depth of the salinity minimum, respectively. The general pattern at the depth of the salinity maximum is warm and relatively salty water associated with the western sectors of the subtropical gyres. The subtropical North Atlantic near-surface salinity field (Fig. 2b) is higher than the other gyres (~36.9), and the North Pacific is the freshest (~34.8). The Indian Ocean near-surface high temperature and salinities are not shifted to the west as in the other subtropical oceans. The Arabian Sea appears as a high near-surface temperature and salinity region.

At the depth of the salinity minimum the highest temperatures (~10.5°C) are observed in the eastern subtropical North Atlantic, the Arabian Sea, and the Madagascar Basin. These three regions are also characterized by higher salinities. The North Pacific is both cooler and fresher than the other ocean basins, consistent with the excess of precipitation at the region of formation of the intermediate waters.

In what follows, the potential for salt finger instability is examined in terms of the distribution of the local density ratios (R_ρ) [Eq. (1)] and goodness of fit (ϵ) [Eq. (4)]. Temperature–salinity diagrams are plotted (Figs. 3–7) at their corresponding geographical location in the depth range between the near-surface salinity maximum and the intermediate waters salinity minimum.

a. North Atlantic

Figure 3 shows the North Atlantic basin's T–S diagram distribution. The density ratio distribution over most of the south and western North Atlantic is characterized by values smaller than 2.0 and a good fit between the observed T–S curve and a constant density ratio T–S curve. Comparison of the R_ρ distribution and Schmitt's (1994b) $E - P$ maps (Fig. 1) suggests a good correlation between low R_ρ and regions of net evaporation. The region of R_ρ higher than 2.0 at 5°N coincides with the region of net precipitation in Schmitt's maps, and the band of lowest R_ρ (~1.6 at 15°N) coincides with the maxima in $E-P$. Here (ϵ) that are smaller than 1.0 are typical over most of the North Atlantic basin.

b. South Atlantic

The South Atlantic T–S diagrams (Fig. 4) resemble Greengrove and Rennie's (1990) distribution, despite the smoothing associated with the Levitus (1982) data. Low R_ρ are observed on the subtropical gyre and high R_ρ are associated with the tropical region. There is some discrepancy with Greengrove and Rennie's (1991) maps particularly in the western sector of the tropical region where their study shows R_ρ higher than 2.0, and the estimates presented here are closer to 1.90.

Greengrove and Rennie (1991) suggested the observed low R_ρ over the Argentine Basin is the result of a combined effect of lateral advection of warm and salty water (Brazil Current) overlying cold and fresh Antarctic Intermediate Water, and of a positive $E - P$ (Hoflich 1984) associated with the subtropical gyre circulation. The overall distribution of low R_ρ values (<2.0) is consistent with this and with our understanding of the AAIW path in the South Atlantic.

With a few exceptions (at 45°S), most likely due to the presence of the subantarctic front, all T–S correlations are better described by a constant density ratio curve than by a straight line ($\epsilon < 1$), suggesting that salt finger instabilities are an active process throughout the South Atlantic.

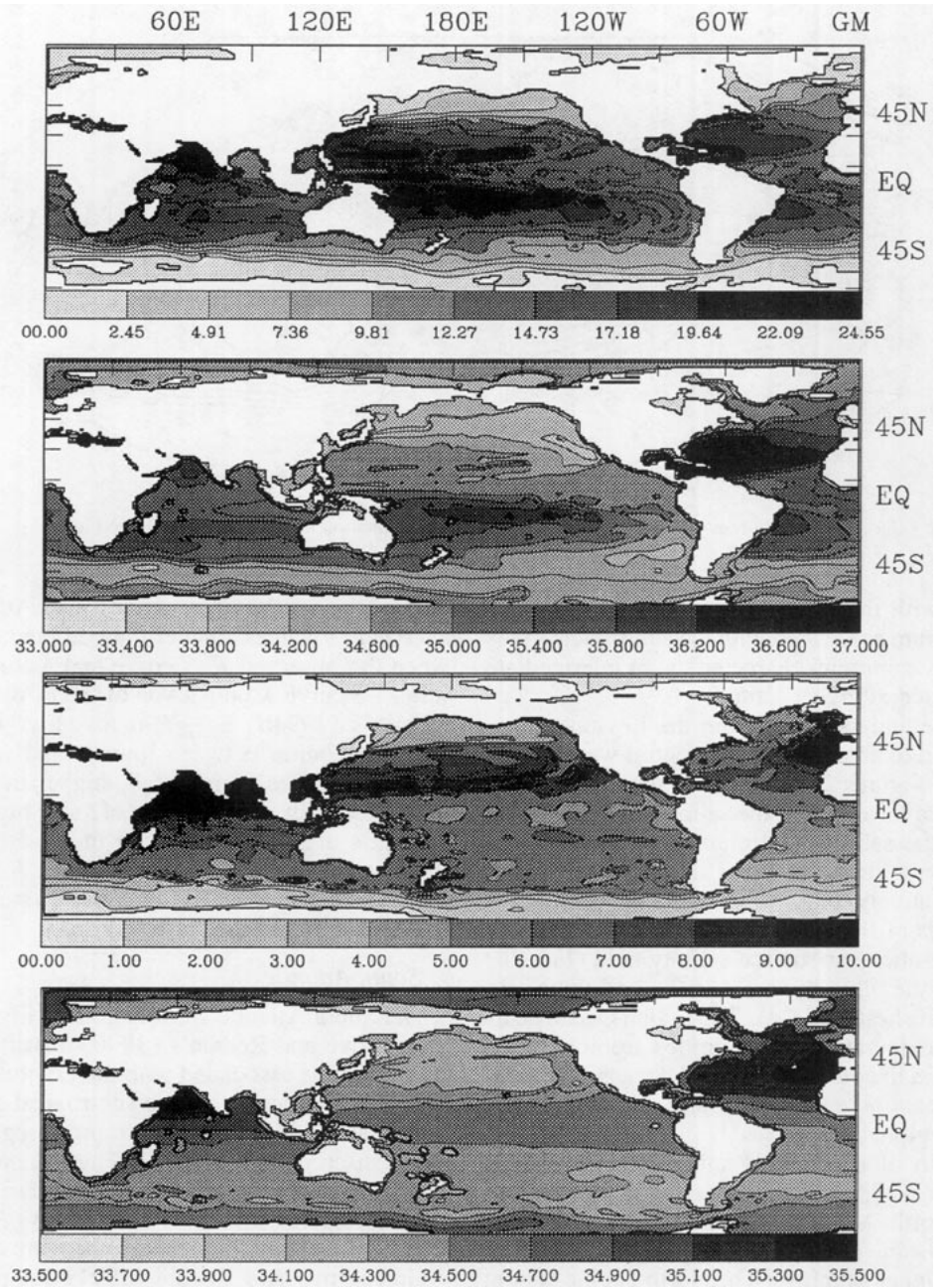

FIG. 2. (a) Temperature and (b) salinity at depth of the salinity maximum. (c) Temperature and (d) salinity at depth of the salinity minimum.

Gordon's (1981) analysis of the South Atlantic Central Water in the region of the Brazil–Malvinas Confluence suggest that salt fingers are the main process responsible for the smoothing of small-scale salinity intrusions observed from CTD casts. According to Gordon, this mechanism results in an enhanced downward salinity flux at middepths, which in turn carries salt to deeper levels to balance the low-salinity subantarctic waters.

c. *North Pacific*

The $E - P$ distribution in this basin (Fig. 1) presents two well-defined regions of net precipitation: the subpolar gyre and the intertropical convergence zone. The relatively weak ventilation of intermediate waters in the northern branch of the North Pacific subtropical gyre (Huang and Bo 1994) and the net precipitation at high latitudes results in relatively fresh intermediate waters

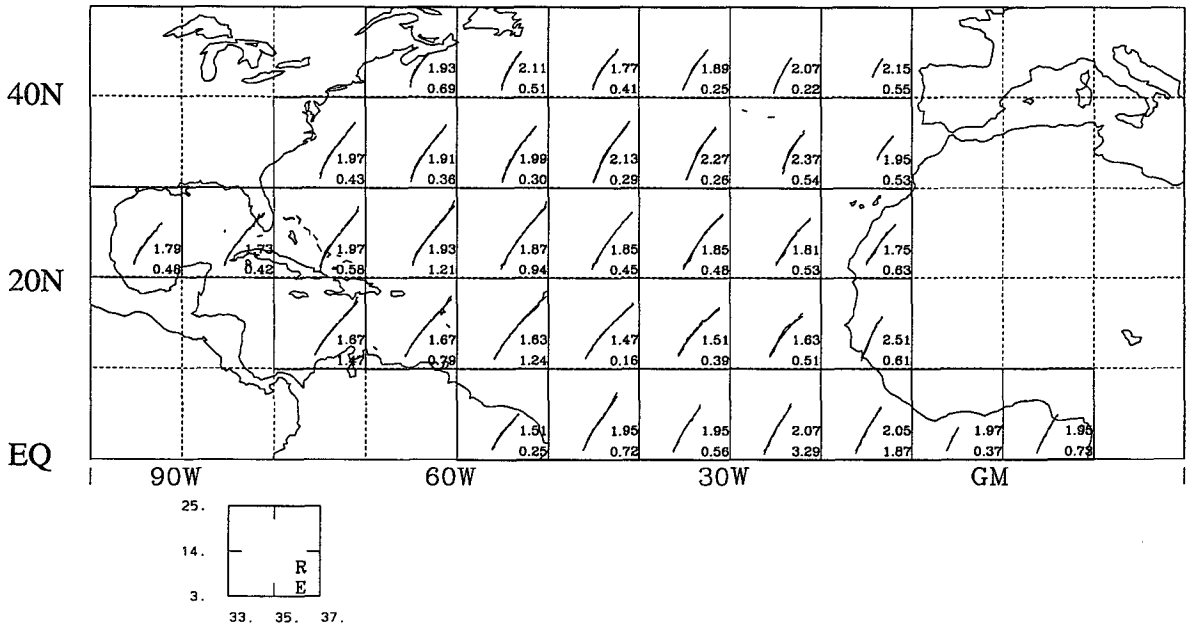

FIG. 3. North Atlantic Central Water temperature and salinity diagram and best-fit constant density ratio curve. Temperature and salinity ranges are 4°–25°C and 33.0–37.0 psu. The upper and lower numbers in each box corresponds to the density ratio and error ratio, respectively.

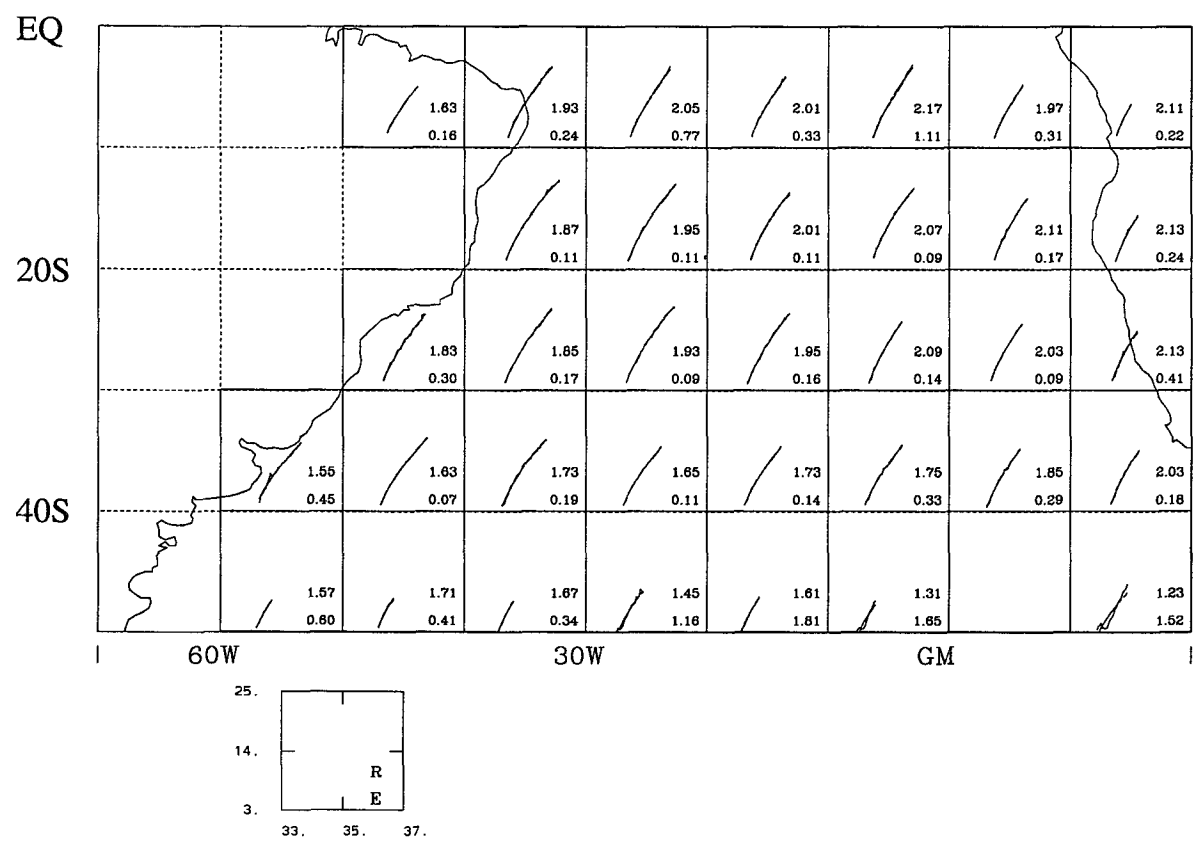

FIG. 4. As in Fig. 2 but for South Atlantic Central Water.

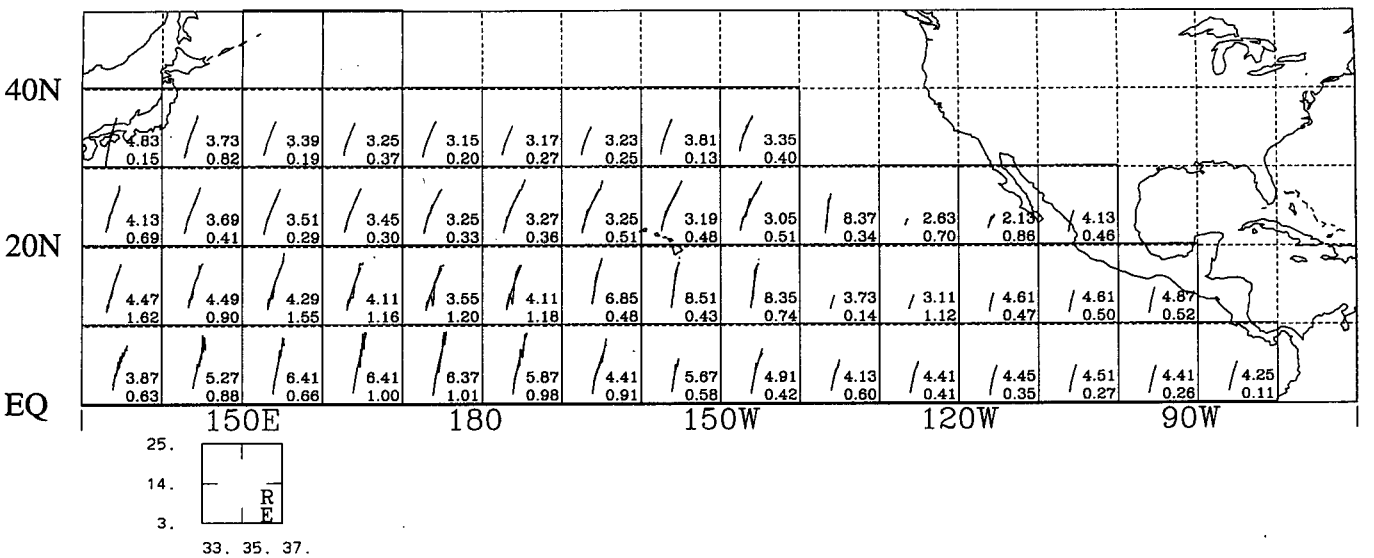

FIG. 5. As in Fig. 2 but for North Pacific Central Water.

and a small salinity difference between the two end-members.

Both near-surface and intermediate waters in the subtropical North Pacific are fresher than the corresponding waters in the other ocean basins (Fig. 2), resulting in $R_\rho > 3.0$ over most of the basin. Density ratios (Fig. 5) south of about 20°N are larger than 5 as a result of the small salinity difference between near-surface and intermediate waters associated with the net precipitation in the intertropical convergence zone. The error ratio (ϵ) distribution is smaller than unity over most of the basin, with some isolated regions with values higher than 1.

d. South Pacific

Net evaporation in the eastern South Pacific and net precipitation in the western Pacific (Fig. 1) results in a somewhat fresher near-surface salinity maxima in the western than in the eastern sector. Consistent with the northward displacement of the intertropical convergence zone the T–S diagrams in the equatorial region

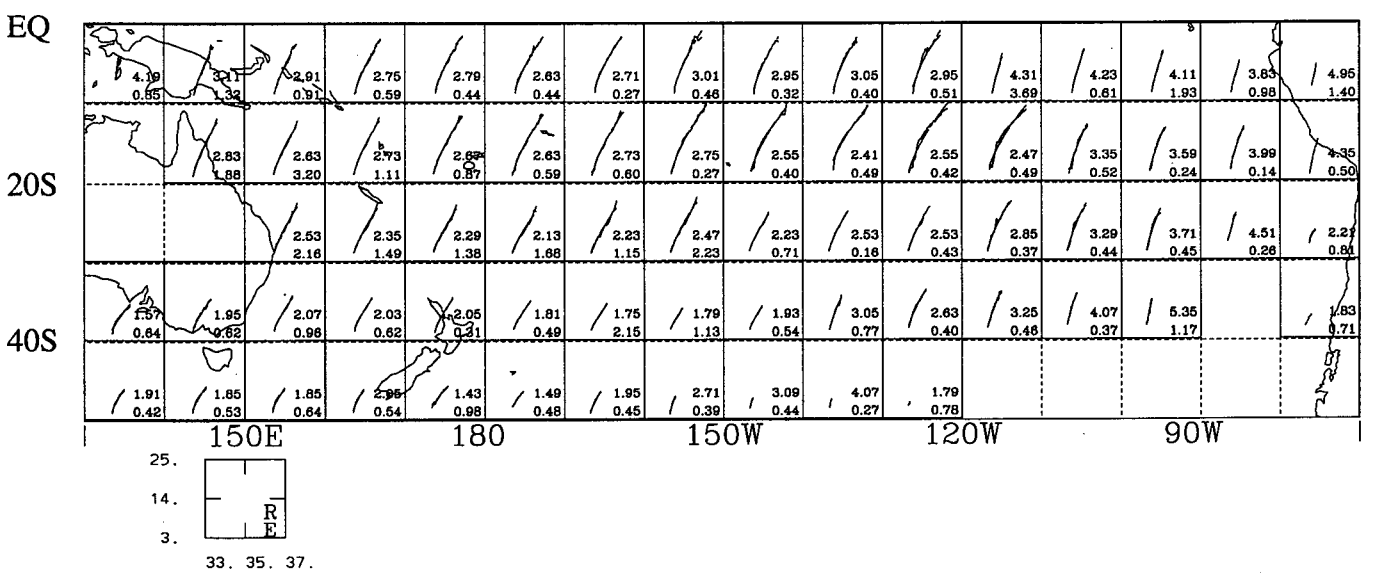

FIG. 6. As in Fig. 2 but for South Pacific Central Water.

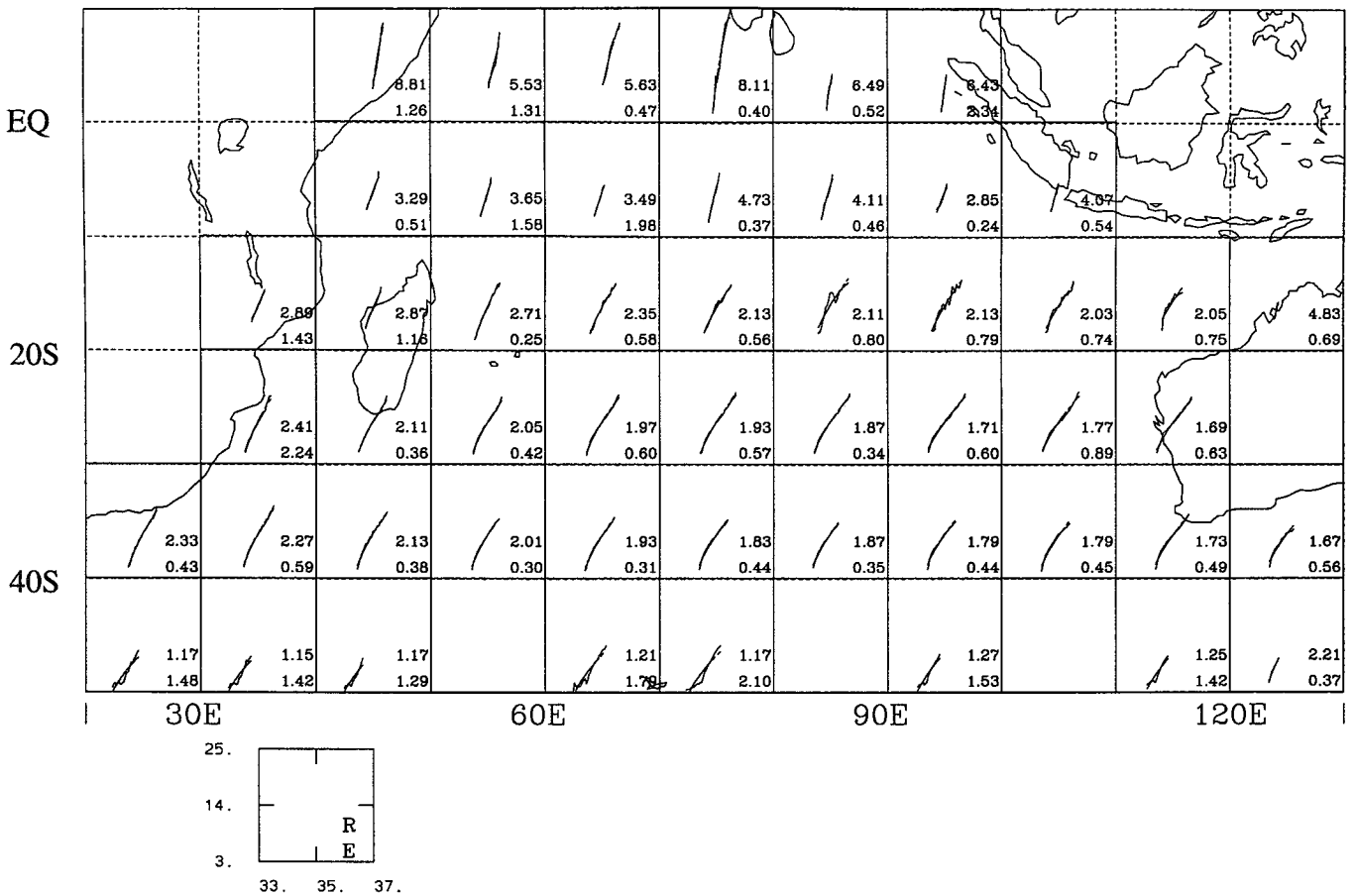

FIG. 7. As in Fig. 2 but for Indian Ocean Central Water.

differ significantly from those in the North Pacific equatorial region. The salinity field at the depth corresponding to the near-surface salinity maxima (Fig. 2b) is in general consistent with $E - P$ distribution: relatively large salinity values in the north and central subtropical gyre and tropical region corresponding to the maximum of net evaporation, and lower salinity values in the western subtropical region and southwestern Pacific.

The AAIW is warmer and saltier than the South Atlantic AAIW (see Piola and Georgi 1982). The input of saltier waters from the Coral Sea increases the salinity of the intermediate waters originating in the region of the Tasman Sea (Piola and Georgi 1982). The southwestern Pacific density ratios (Fig. 6) appear as a continuation of the Indian Ocean distribution. Except for this, the rest of the basin is characterized by $R_\rho > 2.0$.

e. Indian Ocean

The $E - P$ distribution in this basin (Fig. 1) show a region of net precipitation in the northeastern section and a net evaporation in the west and south. The AAIW in the subtropical region of the south Indian Ocean is warmer and saltier than in the South Atlantic and South Pacific (Fig. 2d). Here $R_\rho < 2$ (Fig. 7) are observed in a zonal band extending from about 50°E into the Pacific (Fig. 7).

4. Conclusions

In this paper we estimate the World Ocean's central water density ratio distribution from the Levitus (1982) temperature and salinity climatological dataset and use the form of the temperature–salinity relationship to identify the regions where salt finger instabilities might have a direct effect on the large-scale temperature and salinity distribution. This is accomplished by estimating the goodness of fit of a constant density ratio T–S curve and a linear T–S curve with respect to the observed T–S curve.

Figures 8a–c summarize these results. These figures present the R_ρ and ϵ distribution on $10° \times 10°$ squares, respectively. Figure 8c shows a scatterplot on density ratio–error ratio space. Regions where $R_\rho < 2$ are considered to be susceptible to salt fingers instabilities

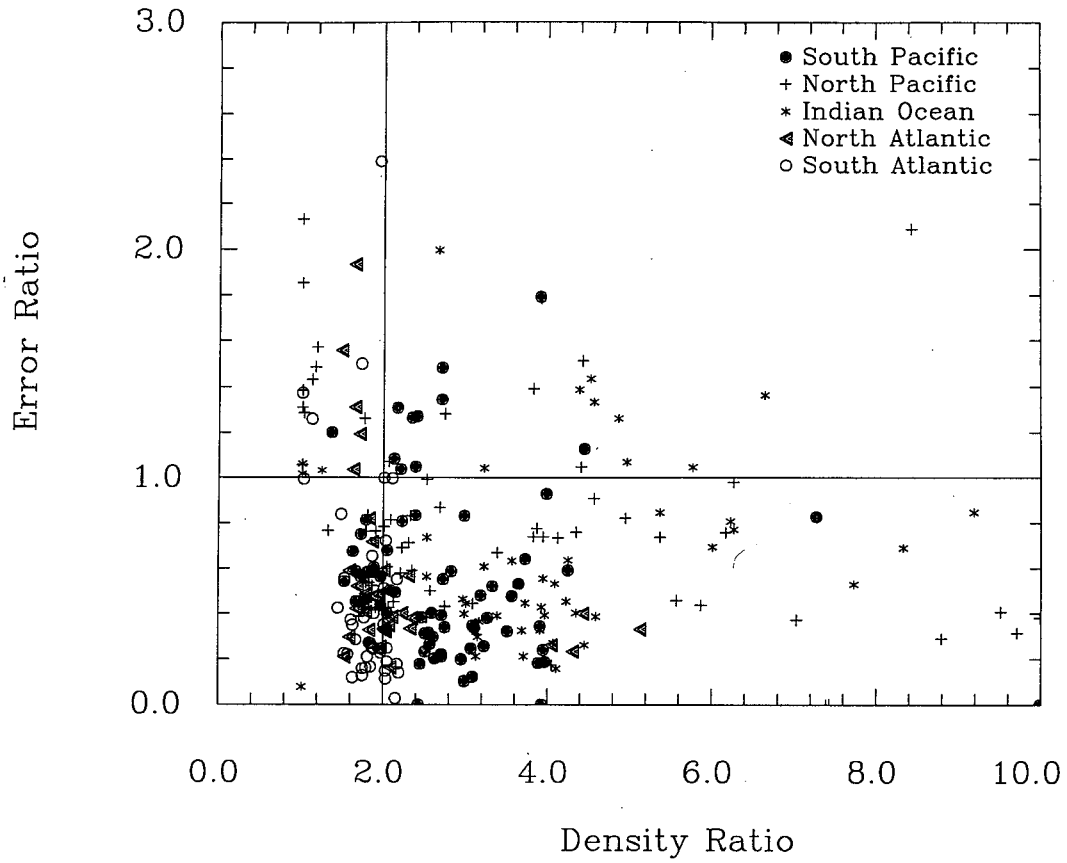

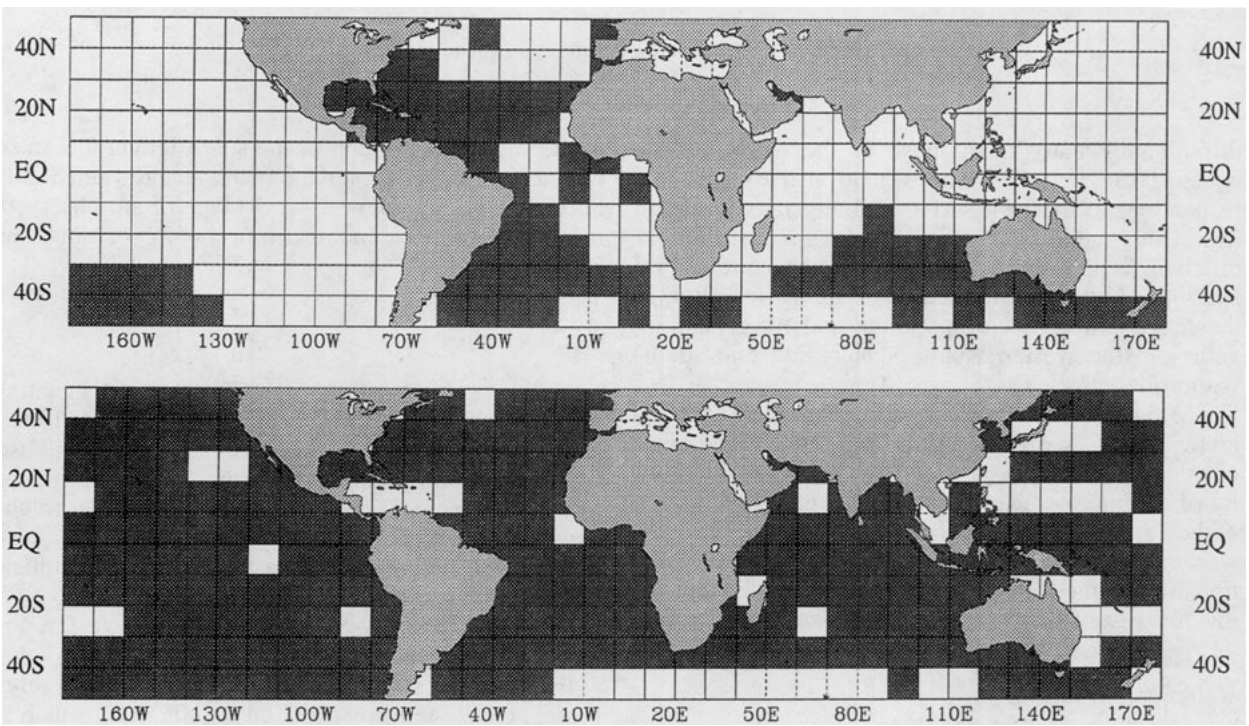

FIG. 8. (a) Scatterplot of density ratio and error ratio (ratio between error associated with a constant density ratio curve fit and a linear fit to the observed T–S curve), (b) Geographical distribution of density ratios. Shading corresponds to $R_\rho < 2$. (c) Geographical distribution of error ratios; shaded areas have $\epsilon < 1$.

(Fig. 8a). Regions where $\epsilon < 1$ indicate that the observed $T-S$ curve is better represented by a constant density ratio $T-S$ curve than by a straight line connecting near-surface and intermediate water types (Fig. 8b).

The maps show the North and South Atlantic, and part of the Indian and southwestern Pacific Oceans, as regions where $R_\rho < 2.0$, suggesting the potential for enhanced vertical salt fluxes due to salt finger. The Indian Ocean, the eastern South Pacific, and all the North Pacific have density ratios between 2 and 10, consistent with the relatively fresher near-surface and intermediate waters. There is in general a relatively good correlation between the regions of net evaporation and low density ratio, and the regions of net precipitation and high density ratio.

The scatterplot in Fig. 8c shows that the Atlantic Ocean density ratio and error ratio estimates are mostly in the area $R_\rho < 2$, $\epsilon < 1$ (Fig. 8a), suggesting this region is susceptible to salt finger instabilities and that the large-scale $T-S$ curve reflect this circumstance.

Most of the ocean's central water $T-S$ relationship appear to be better described by a constant density ratio curve than by a straight line. This is true even in regions where $R_\rho > 2.0$ and enhanced vertical salt fluxes associated with salt finger instabilities would be expected to be too weak to affect the large-scale $T-S$ relationship. The reason for this is unclear. The representativeness of temperature and salinity fields from the Levitus climatology in regions of sloping isopycnals has recently been examined by Lozier et al. (1994). Lozier et al. showed that isobaric averaging (as opposed to isopycnal averaging) of temperature and salinity data as used in Levitus's climatology could result in an unrealistic representation of the actual temperature and salinity fields. However, as suggested by Lozier et al.'s. Fig. 6, isobaric averaging would tend to linearize the averaged $T-S$ curve and therefore tend to increase the number of boxes where a straight line is a better fit to the observed $T-S$ curve. Thus, our estimates do not appear to be significantly influenced by this type of problem.

The result presented here suggests that in addition to turbulent mixing of properties, double diffusive fluxes of temperature and salinity are at play in the ocean and affect the large-scale distribution of properties. Whether consideration of a density ratio dependent diffusivity for heat and salt would solve the deficiencies on the representation of the water mass structure in large-scale GCM is, however, not clear. A first step to answer this question was taken by Gargett and Holloway (1992). They examined the sensitivity a primitive equation ocean model to the use of a different diffusivity for salinity and temperature and concluded that certain large-scale features of the ocean circulation, such as water mass characteristics and magnitude of the thermohaline circulation, were in fact very sensitive to the ratio of the thermal diffusivity to haline diffusivity. However, because of the ideal of their simulations, it is not obvious whether the deficiencies mentioned above were actually solved. This question still needs to be addressed.

Acknowledgments. Comments by two anonymous reviewers were most helpful. This research was supported in part by DOE Grant DE-FG02-90ER61052 and completed under National Science Foundation Grant OCE-94-02633.

REFERENCES

Baumgartner, A., and E. Reichel, 1975: *The World Water Balance.* Elsevier, 179 pp.

Gargett, A. E., and G. Holloway, 1992: Sensitivity of the GFDL Ocean Model to different diffusivities for heat and salt. *J. Phys. Oceanogr.*, **22,** 1158–1177.

Gordon, A. L., 1981: South Atlantic thermocline ventilation. *Deep-Sea Res.*, **33,** 573–585.

Greengrove, C. L., and S. E. Rennie, 1991: South Atlantic density ratio distribution. *Deep-Sea Res.*, **38** (Suppl. 1), S345–S354.

Hoflich, O., 1984: Climate of the South Atlantic Ocean. *World Survey of Climate, Vol. 15, Climates of the Oceans.* H. E. Landsberg and H. van Loon, Eds., Elsevier, 1–192.

Huang, R. X., and B. Qiu, 1994: Three-dimensional structure of the wind-driven circulation in the subtropical North Pacific. *J. Phys. Oceanogr.*, **24,** 1608–1622.

Huppert, H. E., and J. S. Turner, 1981: Double-diffusive convection. *J. Fluid Mech.*, **106,** 299–329.

Ingham, M. C., 1966: The salinity extrema of the World Ocean. Ph.D. dissertation, Oregon State University, 63 pp.

Levitus, S., 1982: *Climatological Atlas of the World Ocean.* NOAA Prof. Paper No. 13 U.S. Govt. Printing Office, Washington DC, 173 pp. and 17 microfiche.

Lozier, M. S., M. S. McCartney, and W. B. Owens, 1994: Anomalous anomalies in averaged hydrographic data. *J. Phys. Oceanogr.*, **24,** 2624–2638.

Piola, A. R., and D. T. Georgi, 1982: Circumpolar properties of Antarctic Intermediate Water and subantarctic mode water. *Deep-Sea Res.*, **29**(6A), 687–711.

Schmitt, R. W., 1981: Form of the temperature-salinity relationship in the central water: Evidence for double-diffusive mixing. *J. Phys. Oceanogr.*, **11,** 1015–1026.

——, 1990: On the density ratio balance in the central water. *J. Phys. Oceanogr.*, **20,** 900–906.

——, 1994a: Double diffusion in oceanography. *Annu. Rev. Fluid. Mech.*, **26,** 255–285.

——, 1994b: The ocean freshwater cycle. JSC Ocean Observing System Development Panel, Texas A&M University, College Station, TX. 40 pp.

——, and D. L. Evans, 1978: An estimate of the vertical mixing due to salt fingers based on observations in the North Atlantic central water. *J. Geophys. Res.*, **83**(C6), 2913–2919.

UNESCO, 1981: Background papers and supporting data on the international equation of state of seawater 1980. UNESCO Technical Papers in Marine Science, **38,** 192 pp.